Experimental Investigation of Fluid Dynamics in a Gravitational Local Recirculation Photobioreactor

Monica Moroni[a]*, Agnese Cicci[b], Marco Bravi[b]

[a]Dipartimento di Ingegneria Civile Edile e Ambientale, Sapienza Università di Roma, v. Eudossiana 18, 00184 Roma, Italia
[b]Dipartimento di Ingegneria Chimica Materiali Ambiente, Sapienza Università di Roma, v. Eudossiana 18, 00184 Roma, Italia
monica.moroni@uniroma1.it

Microalgal and cyanobacterial growth rate does not exert its full potential in high sunlight due to intrinsic limits of the photosynthetic systems that get 'electronically-flooded', thus leading to extensive thermal dissipation and photoinhibition. It is well known, however, that supplying high light in short pulses significantly reliefs this problem and much research is devoted into the development of photobioreactors which exploit this basic feature of photosynthetic systems. The present work deals with an experimental fluid dynamic analysis of the flow developed in a wavy-bottomed cascade photobioreactor for microalgal or cyanobacterial culture. A short but representative section of the equipment was analysed by suspended particle tracers and fast cinematography. The acquired image sequence was post-treated by using a specially designed software implementing the Feature Tracking technique. The effect of the installation and operating mode of the photobioreactor was tested at multiple overflowing liquid flow rates. A local recirculatory zone was found to establish in each trough and its size, local speed, and recirculatory period were characterised as a function of liquid flow rate. Local recirculation establishes owing to gravity only, so that this type of reactor could be rightfully denoted as 'gravitational local recirculation' (GLR) photobioreactor.

1. Experimental Equipment

The core of the experimental set-up is one 120 cm long waved surface made from commercial fiberglass half-processed material, provided with 10 cm high side transparent glass rims, which was installed with the ridges lying on a (virtual) plane inclined with respect to a horizontal plane, as shown in Figure 1.

The waved surface comprises 15 complete vanes (Figure 2). Its bottom surface is connected to a screw jack allowing several inclinations to be set.

The inclination of 6° of this wavy surface reflects those of the 5 m[2] outdoor pilot unit installed at CNR-ISE and described by Torzillo et al. (2010).

The channel is fed via a variable height tank connected to a diffuser installed in the topmost trough of the wavy surface and water is discharged at the exit into an output reservoir. The water level within the tank is controlled through an overflow exit. The average flow rate depends on the hydraulic head at the inlet diffuser. Experiments were conducted at three different elevations of the tank (referred to the inlet diffuser height, which were 0.84 m, 1.84 m and 2.69 m). Table 1 shows the flow rates measured for each height of the tank and the 6° slope of the bottom plate. In the following discussion, we use the symbols Q1, Q2 and Q3 to indicate the inlet diffuser heights as well as flow rates.

Table 1: Flow rates measured for each height of the tank and inclination of 6° (values in l/h)

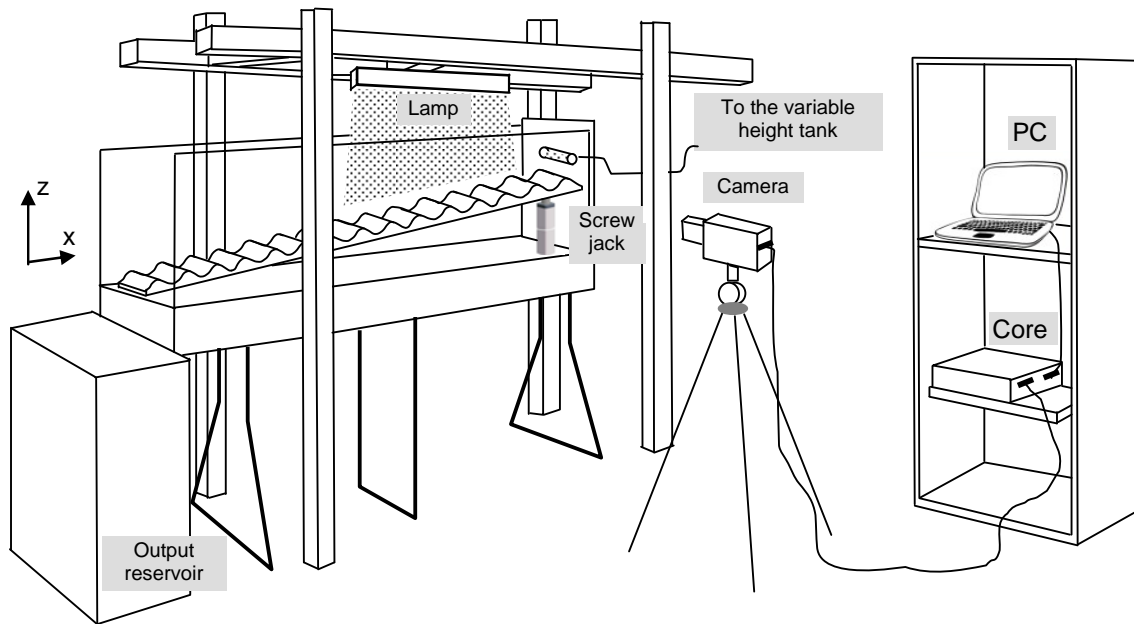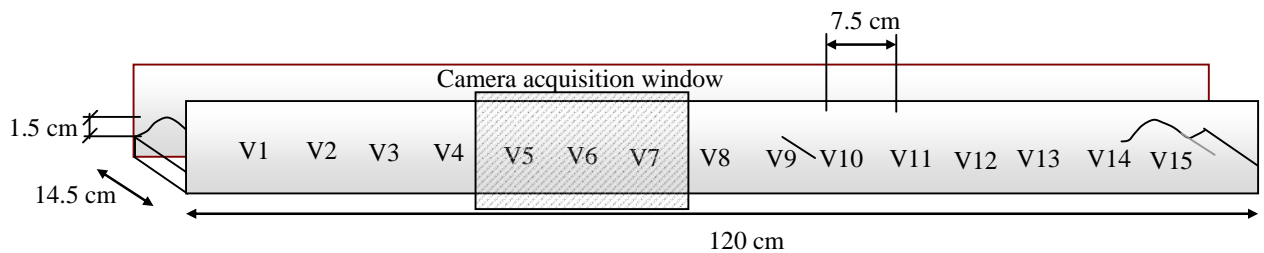| SLOPE	Q1	Q2	Q3
6°	368	490	610

Figure 1: Experimental set-up

Figure 2: Waved surface dimensions

The water was seeded with a well-reflecting passive tracer to allow qualitative visualization of the flow and quantitative estimation of velocity field through image analysis. The seeding particles were yellow-green fluorescent microspheres (Cospheric), with a diameter in the range 53-63 µm.

Proper illumination was ensured through the use of a LED-based Linescan Illuminator (COBRA Slim) installed right above the wavy surface at a distance ensuring that water drop impingement from high turbulence in the channel was minimised (minimisation of light diffusion at source-level), parallel to it, along the middle line of the liquid flow (minimisation of boundary effects from the walls) and close to the lower discharge section (minimisation of boundary effects from the distributor section). A light sheet was thereby generated 40 cm long and 1 cm thick, oriented in the longitudinal direction (i.e., parallel to the mean flow field).

The image acquisition system consisted of two components: a high-speed, high-resolution camera (Mikrotron EoSens) equipped with a Nikon 50 mm focal length lens; the camera captures gray-scale images at up to 500 fps with a resolution of 1280x1024 pixels (for the present set of measurements, images were acquired at 400 fps) and a high-speed Camera Link digital video recorder operating in Full configuration (IO Industries DVR Express® Core) to manage data acquisition and storage. The captured image flow was transferred to a personal computer under the control of the DVR Express® Core software. The camera acquisition window framed 3 vanes of the wavy-bottomed cascade photobioreactor (gray shaded area in Figure 2). A two-dimensional orthogonal reference system (x-z), where x is the horizontal axis (positive upslope) and z is vertical axis (positive upward), is introduced. The origin of the reference system is set in correspondence of the image left bottom corner. One camera and a planar light sheet are the basic requirement for the application of a two-dimensional image analysis technique.

The whole apparatus described thereupon was enclosed in a dark room made by a thick dark plastic sheet to minimise light interference from external sources.

The duration of each experiment was approximately 60 s, i.e., the time required for the tracer particles introduced in the topmost trough of the wavy surface to pass through the test section.

2. Image Postprocessing

The trajectories of tracer particles seeding the fluid were reconstructed and the velocity field evolution over time was identified by means of Feature Tracking (FT), a particle tracking algorithm that permits to ignore the constraint of image low seeding density (Raffel et al., 2007). This algorithm can provide accurate displacement vectors even when the number of tracer particles within each image is very large (Moroni and Cenedese, 2005). FT reconstructs the displacement field by selecting image features (image portions that are suitable for tracking because they remain almost unchanged over small time intervals) and tracking those from frame by frame. The matching measure used to follow a feature (and the LxH window around the feature, where L and H are the horizontal and vertical dimensions, respectively) and its "most similar" region at the successive times is represented by the "Sum of Squared Differences" (SSD) of the intensity values.

The displacement is defined as the one that minimizes the SSD. In Feature Tracking, the algorithm is applied only to points for which the solution for the displacement exists; those points are called "good features to track". FT allows a Lagrangian description of the velocity field that provides sparse velocity vectors with application points coincident with large luminosity intensity gradients, which are likely located along tracer particle boundaries (Shindler et al., 2012).

Post-processing and presentation of experimental data are extremely important in representing and understanding flow behavior. Moreover, the post-processing method ultimately determines the accuracy of the information extracted from the velocity vectors. The interpolation step is necessary to map randomly spaced Lagrangian data onto regular grids, i.e., to produce instantaneous or time-averaged Eulerian velocity fields, to replace erroneous vectors with values computed from the neighboring vectors or to refine the original grid. The interpolation step, due to the low-pass filtering process, determines the loss of the high frequency flow characteristics (Moroni et al., 2008).

The mean velocity components along axes x and z, u and w, are evaluated in the knots of a regular grid of 60 rows and 256 columns (cell sizes of about 1x1 mm^2). Assuming the phenomenon is stationary as well as ergodic, the ensemble averages are evaluated as temporal averages over a time interval equal to the entire recording time of about 24000 frames.

3. Results and Discussion

The particle trajectories allow a qualitative description of the flow field main features.

Figures 3 (a) and (b) present a sample of the processed experimental results showing the velocity vectors overlapped with the color map of the horizontal and vertical velocity components, respectively, for the maximal flow rate (Q3). Figure 3 (c) presents the streamlines that show the characteristic average behavior of the fluid flowing through the photo bioreactor (PBR). Two regions can be easily visualised: a principal current flows close to the channel bottom and one recirculation area in clockwise motion establishes in each vane close to the current free surface.

After determining the velocity field, all the potential sources of high frequency light-dark alternation within the troughs of the photobioreactor exposed to sunlight were spotted and analysed by using the velocity fields themselves.

Two major sources were identified: 1. the recirculatory area, where a significant portion of the entrapped liquid circulates (theoretically, all but the stationary center) and is exposed to different illumination intensity due to Lambert-Beer intensity reduction as a function of depth in the liquid; 2. the liquid stream flowing close to the wavy bottom, i.e., again, alternatively, close to the liquid surface or below a thick liquid layer and, therefore, exposed at varying illumination regimens.

For the recirculatory area, the recirculation time was determined. For this purpose, by following the vertical line passing through the center of the vortex, a velocity plot was created (Figure 4) beginning from the top surface of the liquid down to the trough bottom. A positive value of velocity in the plot indicates that local velocity is oriented upstream, a negative value means that the velocity vector is oriented downstream.
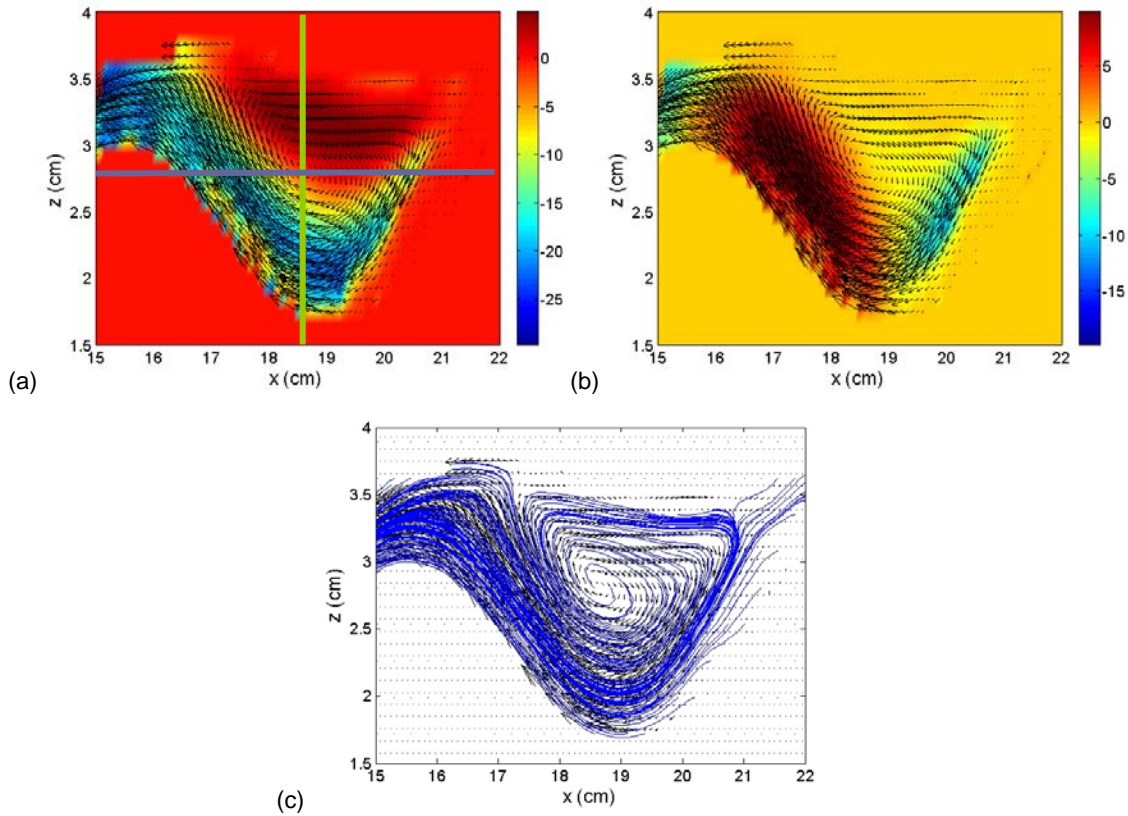
(a)

(b)

(c)

Figure 3: Velocity vector field at the maximal flow rate overlapped with (a) the color map of the horizontal velocity component; (b) the color map of the vertical velocity component; (c) the flow streamlines. The lines indicate the profiles passing through the center of the vorticose zone for velocity plot creation
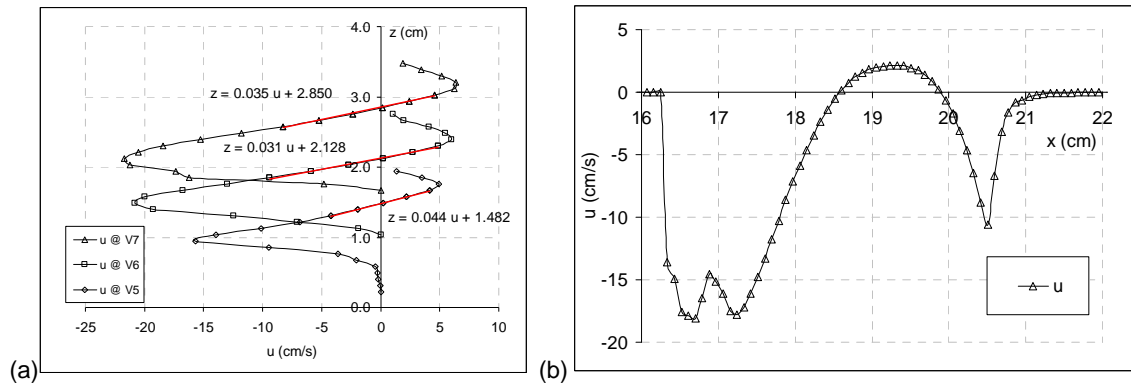

(a)

(b)

Figure 4: (a) Vertical and (b) horizontal sectional views of the velocity field for all points along the vertical and horizontal profiles drawn through the vortex center in Figure 3 (a)

Three profiles are reported, from which a consistence of the shapes of absolute values of velocity among the three troughs can be noted. The three profiles exhibit a vertical displacement with respect to each other in the plot, which is due to the different elevation of the three troughs, in turn consequent to the inclination of the wavy bottom.

Each profile starts at the liquid-air interface with a positive velocity. First velocity increases with increasing depth, determining a velocity difference higher than expected, and then decreases down to the center of the vortex, where it becomes null. The velocity profile then increases in the negative direction up to an absolute value which is higher than the maximum in the positive direction. This region is relevant to the

stream flowing next to the bottom of the channel and does not recirculate but, rather, flows directly to the next trough by overpassing the curved weir.

Within each plot, a reasonably linear zone can be noted (marked in red along each curved profile), which indicates that the gradient is constant within a relatively ample zone; this zone indentifies the recirculating zone, which thumbles as if the whole liquid volume rolled as a rigid body. By considering the value of the velocity gradient within the vortex, $(\partial u/\partial z)$, we can write the recirculation period (t_c) of the liquid elements within the thumbling volume:

$$t_c = \frac{2\pi r}{\frac{\partial u}{\partial z} r} = \frac{2\pi}{\frac{\partial u}{\partial z}} \tag{1}$$

where r represents the characteristic dimension of the vorticose structure. The profiles of horizontal velocity component along the cross-section passing through the vortex center drawn in Figure 3a were also used to calculate the characteristic horizontal and vertical sizes of the vortex structure (d_V and d_H). Using the vertical "cut" through the vortex center, d_V was taken as twice the distance between two subsequent points where the velocity profile assumes the zero value. Similarly, d_H was taken as twice the distance between two points in the profile of local horizontal velocity where such velocity becomes zero. One should consider that the vortex center has zero velocity in both the vertical and horizontal directions; therefore three zeros are required to brace the vortex characteristic sizes.

Table 3: Sizes of the vortex zone and local recirculation time in the three tested flow rate conditions

H	q (L/h)	Recirculation time (s)	Vertical size (cm)	Horizontal size (cm)
3	610	0.230	1.449	2.536
2	492	0.327	1.339	1.786
1	371	0.389	0.532	1.774

As far as the non-recirculating stream, it can be seen that velocity reaches a very large value within its core and then velocity decays to zero. From Figure 4, it can be observed that the average value of velocity within the core of this stream is approximately 60% higher than the maximum (peripheral) local velocity of the thumbling volume. By assuming, conservatively, that velocity will be exactly equal to said peripheral velocity and will be invariant during flow, we can calculate the free-flowing stream period to be the ratio between the curved path from one ridge to the next to the flow velocity itself. By taking the ratio, the results shown in Table 4 are obtained.

Table 4: Ridge-to-ridge travel time in the non-recirculating area for the three tested flow rate conditions

H	q (L/h)	Travel time (s)
3	610	0.361
2	492	0.413
1	371	0.572

Microalgae entrapped in recirculating volumes experience a dark-light sequence for reasonably concentrated suspensions. For the geometry under test, this occurs for an optical density of the suspension equal to 3.5, i.e. 3 to 8 g/L of microalgae. At noon, the external revolving layer will experience full light exposure at the top, and full darkness at the bottom, that is a 1:1 ratio. The revolving layers closer to the revolution axis will enjoy a milder illumination variation (a lower maximum intensity and a higher minimum intensity), corresponding to a longer (e.g., 2:1) light:dark sequence. Conversely, when the radiation intensity is lower (e.g. early morning or sunset), the external revolving layer will fall below the compensation intensity well above the bottom point, corresponding to a shorter (e.g., 1:2) light:dark sequence, while revolving layers closer to the revolution axis may benefit from a 1:1 ratio. Here, we sticked to the consideration that all the revolving material is subjected to the (average) 1:1 sequence at the calculated frequency, which is reasonably independent of suspension concentration. Moreover, the shallow suspension layer flowing along the wavy surface bottom was assumed to share the same light exposition intensity and the same 1:1 light:dark ratio. According to Grobbelaar (2006), for a 1:1 duty cycle in illumination, fast light-dark alternation results in a photosynthetic activity which can be estimated by:

$$PA = 281.7 - 16.3 \cdot \ln(t) \qquad (2)$$

where PA is photosynthetic activity and t is the light-dark alternation time.

The values reported in Table 5 were calculated based on the revolution periods given in Tables 3 and 4 using Eq. (2), the reference case being a 1 s recirculation time PBR.

Table 5: Estimate of photosynthetic activity increase due to fast light-dark alternation in the wavy photobioreactor at the different tested flow rate conditions

H	q (L/h)	Recirculatory Area	Non-recirculatory area
3	610	9%	6%
2	492	6%	5%
1	371	5%	3%

This photosynthetic activity increase is expected to directly make into a correspondingly higher specific growth rate, hence increased biomass production, with respect to photobioreactors operated under moderately fast mixing conditions.

The estimates calculated here should be intended as a first approximation, as Grobbelaar's research results that we are leveraging were obtained on two specific microalgae (*S. obliquus* and *Chlorella* spp.). The directions for the further development of this research include carrying out experiments to highlight actual improvements on specific microalgal species and characterising this unit at higher flow rates (1000 L/h). Our previous estimates with a simpler experimental technique showed that there may be room for a further reduction of the recirculation time, although the applicability of the experimental technique described in this article with the present setup may be impaired by air bubbles entrainments taking place at higher flow rates (because of the reduced intensity of the light passing the liquid surface and the reduced applicability of the feature tracking algorithm).

Furthermore, any expected productivity increase is relevant to the illuminated portion of the photobioreactor volume, and should therefore be proportionately reduced by the dark fraction of the overall volume (e.g., the pumping circuit which is required to recirculate the biomass to the top of the apparatus).

4. Conclusions

By carrying out a fast-cinematography fluid dynamic study with tracers on a wavy-bottomed photobioreactor at various liquid flow rates, and then by applying specific algorithms to the experimental results, the velocity field was determined and free-flowing and extensive recirculatory areas were identified. By elaborating these results, the recirculation period and all periods expected to result in light-dark alternation (the so-called "flash effect") were determined along with the expected productivity increase. The local recirculation establishes owing to gravity only, so that this type of reactor could be rightfully denoted as 'gravitational local recirculation' (GLR) photobioreactor.

References

Grobbelaar, J.U., 2006. Photosynthetic response and acclimation of microalgae to light fluctuations. In: Algal cultures analogues of blooms and applications. Science Publishers, Enfield, NH, USA, 671--683.

Kok B., 1953. Experiments on photosynthesis by *Chlorella* in flashing light. In: Burlew B (Ed.) Algal Culture: From Laboratory to Pilot Plant. Carnegie Institution of Washington Publication 600, Washington, DC, 63–158.

Moroni M., Kleinfelter N., Cushman J.H., 2008. Alternative Measures of Dispersion Applied to Flow in a Convoluted Channel. Advances in Water Resources, 32(5), 737-749.

Moroni M., Cenedese A., 2005. Comparison among feature tracking and more consolidated velocimetry image analysis techniques in a fully developed turbulent channel flow Measurement Science and Technology, 16, 2307-2322.

Raffel M., Willert C., Werely S., Kompenhans J., 2007. Particle Image Velocimetry, A Practical Guide. Springer, Berlin, Germany.

Shindler L., Moroni M., Cenedese A., 2012. Using optical flow equation for particle identification and velocity prediction in particle tracking. Applied Mathematics and Computation, 218, 8684–8694.

Torzillo G., Giannelli L., Verdone N., De Filippis P., Scarsella M., Martínez-Roldán A. J., Bravi M., 2010. Microalgae Culturing in Thin-layer Photobioreactors. Chemical Engineering Transactions, 20, 265–270.